Electrochemical oxidation of gallic acid: A reexamination of the reaction mechanism in aqueous medium

Abhishek Kumar, Nada Alami-Mejjati, Marcel Bouvet, Rita Meunier-Prest

Graphical abstract

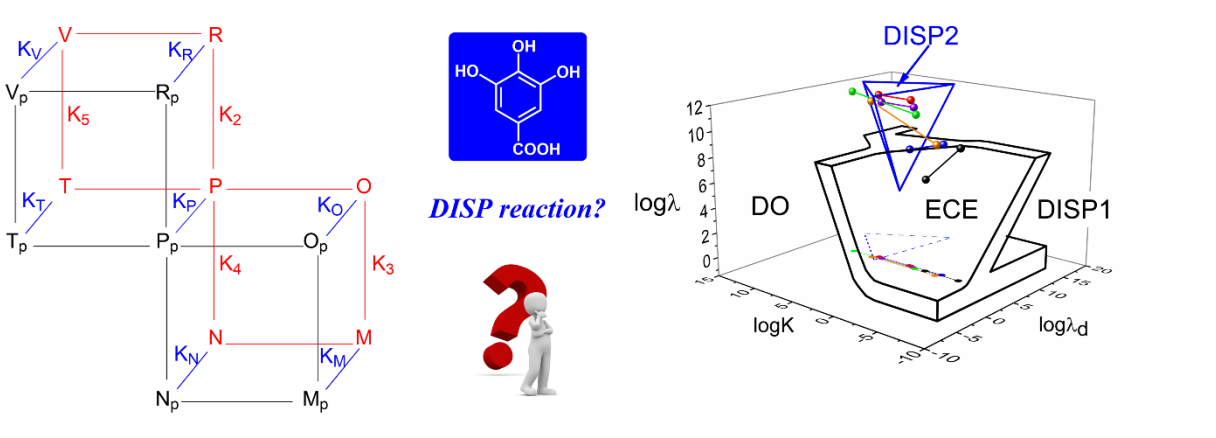

- Oxidation of gallic acid (GA) on gold electrode is examined in a broad pH range.
- Oxidation mechanism of GA based on bi-cubic scheme is proposed.
- pKa value of the final ortho-quinone product is experimentally determined.
- Spectroelectrochemical studies identify the different intermediates and the products.
- The kinetics of gallic acid redox process involves a disproportionation reaction.

Electrochemical oxidation of gallic acid: A reexamination of the reaction mechanism in aqueous medium

Abhishek Kumar, Nada Alami-Mejjati, Marcel Bouvet, Rita Meunier-Prest*

Institut de Chimie Moléculaire de l'Université de Bourgogne, UMR CNRS 6302, Université de Bourgogne, 9 Avenue Alain Savary, Dijon Cedex 21078, France

---

Email addresses and ORCID number of authors (corresponding authors emails are marked with asterisk)

Abhishek.Kumar@u-bourgogne.fr (ORCID no. 0000-0002-4306-9644)

Marcel.bouvet@u-bourgogne.fr (ORCID no. 0000-0002-2272-6633)

*Rita.Meunier-Prest@u-bourgogne.fr (ORCID no. 0000-0001-5597-3879)

Abstract: A clear understanding of redox mechanism of antioxidants, like gallic acid (GA) is important to decipher their radical scavenging functioning in the biochemical environment of the body. Herein, electrooxidation process of GA is reexamined in an aqueous medium through a combination of cyclic voltammetric and spectroelectrochemical studies on gold electrode in wide pH and concentration ranges. These studies reveal redox process of GA as an irreversible two electrons process, resulting in the formation of ortho-quinone, where the second electron transfer is the rate limiting step. The redox process of GA at different pH is presented in the form of a bicubic scheme and the associated thermodynamic parameters are analyzed using Laviron's theory. It allows for the first time the determination of the acidity constant of the corresponding ortho-quinone (pK_a = 5.33). The number of exchanged electrons and protons depends on the pH conditions, such that ($2e^-$, $2H^+$) are exchanged at pH < 4.24 and pH > 5.33, while ($2e^-$, $1H^+$) are exchanged at 4.24 ≤ pH ≤ 5.33. A careful analysis using the theoretical treatment proposed by Amatore and Saveant for an ECE-DISP mechanism demonstrates the existence of a DISP2 mechanism leading to the formation of ortho-quinone through disproportionation of the semiquinone radicals, made possible thanks to their stabilization.

Keywords: Cyclic voltammetry, cubic scheme, disproportionation, quinone, hydroquinone, buffer medium.

1. Introduction

Gallic acid (GA), chemically known as 3,4,5-trihydroxylbenzoic acid is a naturally occurring polyphenol, which is mainly derived from plants, such as tea leaves, grapes, pomegranate, berries and honey among others [1, 2]. It is reported to be highly beneficial for the human bodies because of its anti-microbial [3], anti-carcinogenic [4], anti-mutagenic [5] and anti-inflammatory [6] properties. It performs many important biological functions in the human body and is readily absorbed. Its anti-oxidative properties, which are stronger than these of the other similar antioxidants, such as Trolox, are highly appealing [7]. For instance, it plays a pivotal role in reducing oxidative stress in the body by neutralizing reactive oxygen species (ROS), which otherwise bind to the key biomolecules in body, like proteins, fatty acids and DNA. The phenolic protons in GA are highly reactive to bind with ROS, like OH and OOH radicals, thereby neutralizing them. Because of such advantages, GA based products are often taken as herbal and pharmaceutical supplements. Despite these benefits, overconcentration of GA in the body is reported to be dangerous because of its tendency to bind with macromolecules in the body, like DNA and proteoglycans [8]. Moreover, GA content in many natural products and beverages is considered as a benchmark for their quality. Therefore, monitoring of GA concentration is often necessary to evaluate quality of GA containing products.

Different analytical techniques based on chromatography [9], flow-injection chemoluminescence [10], spectrophotometry [11] and electrophoresis [12] have been reported to determine GA at low concentration. However, complexities in the measurements and high expenditure of these methods make electrochemical approaches a suitable alternative, which are rather cheap, rapid and miniaturizable [13]. Moreover, the presence of three hydroxyl groups and one carboxylic group in gallic acid make it highly electroactive, making electroanalytical methods appropriate for its assessment. Indeed, different electrochemical methods based on voltammetry, amperometry and coulometry have been previously reported

for GA determination [14, 15]. Conventionally, screen-printed carbon and glassy carbon electrodes (GCE) were used to analyze GA, where it is oxidized at more positive potential with a broad anodic wave. To improve the analytical performances, mainly sensitivity and limit of detection (LOD), different electrode modifiers, mainly based on carbon nanomaterials were also used. Multitude of studies on carbon nanotube and related composites modified GCE were reported, exhibiting high sensitivity, low interference and LOD down to a few nM or sub-nM [16-19]. Besides carbon nanomaterials, gold nanoparticles modified carbon paste electrode and silver nanoparticles modified GCE were also reported to detect GA with high analytical performances in food samples [20, 21]. Elsewhere, hybrid materials based on metal organic frameworks and nanoparticles [22, 23] were also used as electrode modifiers on carbon electrodes for voltammetric determination of GA.

The aforementioned studies undoubtedly established the efficiency and reliability of electrochemical approaches in the sensitive detection of GA. However, limited attention has been given to understand the redox mechanism of GA on conventional electrodes, which is pertinent for a suitable electrode design. The electrochemical oxidation of GA in aqueous medium was mechanistically investigated by some researchers previously, mainly on carbon electrode. A few studies proposed a quasi-reversible $2e^-$, $2H^+$ mechanism [24, 25] or a two-step process involving the transfer of a proton and an electron in each step, forming semiquinone radical at first, which is finally converted into ortho-quinone [26]. On the other hand, some studies suggested an ECEC first order mechanism, in which all the reactions are irreversible [27]. However, no consensus could be reached on the proposed reaction mechanism of GA. It is worth noting that in the latter case, the authors provided insufficient evidences to support their claim of the ECEC mechanism, which were only the comparison of one cyclic voltammogram with the digital simulation of an ECEC mechanism. However, changes of the scan rate and of the concentration in GA, which can have significant effect in ECEC

mechanism, were not taken into account. Although, these experiments were performed in the pH range of 1.55-6.22, but they did not explain the distribution of different species with known pK_a values [28-30] within the studied pH window. However, it has to be noted that proton dissociation has a significant impact on the reaction mechanism [31-35]. Moreover, all these measurements were conducted in buffer medium where proton transfer is assumed to be rapid and at equilibrium [36], whereas the authors proposed irreversible deprotonation reactions. This has been well discussed, especially for redox systems similar to GA, such as benzoquinone/hydroquinone [37] or catechols [38, 39] studied in buffer solutions. In those conditions, the redox process takes place by proton coupled electron transfer (PCET) reaction [36] involving changes in the protonation state of the molecule. Such reactions can be described using a square scheme [31, 32] or a combination of square schemes such as nine-member, cubic or bicubic schemes as reported previously by Laviron and coworkers [33-35].

In this endeavor, the present work aims at exploring the oxidation mechanism of GA in a wide pH range and determining different thermodynamics parameters in the light of Laviron's theory. Beside elaborating redox mechanism of GA, another key novelty aspect is the determination of pK_a of ortho-quinone for the first time, resulting from the oxidation of GA. To achieve these objectives, our strategies involve analyzing the cyclic voltammograms of GA on conventional gold disc electrode in a wide range of scan rate and GA concentrations. Moreover, these measurements are performed in a wide pH range to understand the different electron and proton transfer steps during the GA redox process. In depth, spectroelectrochemical studies are also performed to identify different chemical species formed during the redox process of GA at different pH and concentrations. On the experimental data, different analytic diagnostics have been performed, utilizing the theoretical treatment proposed by Amatore and Saveant for an ECE-DISP mechanism to obtain kinetics and thermodynamics

parameters [40]. Based on these studies and the analytical treatment, finally, the redox mechanism of GA is presented.

2. Experimental

2.1. Chemicals and Reagents

All chemicals used in the experiment were used as received. 3,4,5-trihydroxybenzoic acid; GA (CAS No. 149-91-7; purity/ 97.5-102.5% (titration)), acetic acid (CAS No. 64-19-7; purity ≥ 99.7%), boric acid (CAS No. 10043-35-3; purity ≥ 99.5%) and phosphoric acid (CAS No. 7664-38-2; 85% wt in H_2O) were purchased from Sigma-Aldrich. KNO_3 (CAS No. 7757-79-1; purity: 99.0%), absolute ethanol (CAS No. 64-17-5) and NaOH (CAS No. 1310-73-2; purity: 98.0% anhydrous) were bought from Carlo Erba. The gold disk electrode used in this study (diameter: of 1.6 mm) was bought from Bioanalytical Systems (BASi).

2.2. Electrochemical setup and measurements

Electrochemical experiments were performed on a PGSTAT302N or a µAUTOLAB III workstation from Metrohm, utilizing a conventional 3-electrodes cell, which includes gold disk (1.6 mm or 40 µm diameter), Pt and Calomel (KCl sat.) as working, auxiliary and reference electrodes, respectively. Potentials are reported versus SCE. Cleaning method of the gold electrode includes soaking for 10 minutes in 2 M KOH at first, followed by polishing with 0.05 µm alumina slurry, then chemical etching for 10 minutes in dilute 2 M sulfuric acid and finally sonicating for 5 minutes in water and ethanol mixture. The electrode was then dried with a flow of dry N_2. To finish, the electrode was rinsed with 5 mM phosphate buffer and 50 mM NaCl. Britton-Robinson (BR) buffer solution was prepared by mixing 0.04 M acetic acid, 0.04 M boric acid and 0.04 M phosphoric acid. 0.2 M KNO_3 solution in BR buffer was used as supporting electrolyte. In each buffer, the pH was adjusted to the desired value by addition of 1 M NaOH. A stock solution of 0.02 M GA in absolute ethyl alcohol was prepared, which was

used for different studies during a day. Cyclic voltammograms were recorded in BR buffer/EtOH (v/v: 97.5/2.5), at different pH, for scan rates varying from 10 mV to 400 mV s^{-1} in a potential window 0 to 1.1 V. In each measurement, BR buffers were deoxygenated for 10 minutes with argon and a positive overpressure of argon was maintained above the electrolyte during the measurement duration. All measurements were performed at room temperature (19 ± 2°C).

2.3. Spectroelectrochemical studies.

In situ spectroelectrochemical experiments were performed on a SP-200, BIOLOGIC potentiostat based workstation, using BioLogic cell having an optical path of 1 mm. In the experiments 2 mM GA was used as redox probe in BR buffer + 10 % EtOH. The working, reference and auxiliary electrodes were a gold grid, Ag/AgCl in NaCl (3 M) and a Pt wire, respectively. *In situ* UV-visible spectra were recorded every 3.2 seconds by a UV-visible diode array spectrometer (SEC 2000, BIOLOGIC) using the software Visual spectra 2.1, running in the kinetic mode with an external trigger. The excitation source in the spectrometer was 150 W Xe lamp, which was connected to the cell by optical fibers.

3. Results and discussion

3.1. Electrochemical process of GA on Au electrode

The electrochemical oxidation of GA was investigated by CV cycling in pH range from 1.8 to 7. At pH higher than 7, GA is not stable and decomposes. Fig. 1 depicts the comparison of voltammograms obtained at different pH, exhibiting one anodic wave in the forward scan associated to the formation of ortho-quinone [24, 26], while the absence of any cathodic wave during the reverse scan. It confirms the irreversible oxidation of GA on gold electrode. Moreover, peak potential associated to the oxidation process shifts to more positive values as the pH decreases, as already reported.[26] Notably, no reduction peak was observed irrespective

of the scan rate variation in the range of 10 to 400 mV s^{-1}, contrary to that was observed on glassy carbon electrode where a small reduction peak appeared in the reverse scan. [25, 26] This is attributed to the following chemical reactions, such as dimerization or oligomerization after the electrochemical step [41]. The evidence of a chemical reaction is further provided by recording successive CV cycles at a given pH (Fig. 1b), displaying decrease in the anodic current and positive shift in the oxidation peak of GA as a function of increasing CV cycles. Moreover, emergence of a new anodic wave (noted with a star in Fig. 1) increasing in intensity with the successive CV cycles is also noticed. Such observations clearly indicate that redox process of GA is hindered and a part of the electrode surface is covered by the oxidation product of GA, inhibiting the arrival of GA on the electrified electrode. Therefore, a careful cleaning of the electrode is done before each CV.

Figure 1

The variation of peak potential (Ep) of the voltammograms with pH is further analyzed and its evolution with increasing pH is depicted in Fig. 2. From the plot, a continuous lowering of the Ep in a linear fashion with increasing pH is evidenced, but with three different slopes. Accordingly, a slope value of - 55 ± 2 mV/pH unit for pH ≤ 4.24, - 27 ± 2 mV/pH unit for 4.24 ≤ pH ≤ 5.33 and - 64 ± 4 mV/pH unit for pH ≤ 5.33 are obtained, attesting the release of protons during the oxidation process of GA. For a redox reaction involving the transfer of *n* electrons and *m* protons, the Ep obeys the following equation:

$$\frac{\partial E_p}{\partial pH} \sim const - 2.303\frac{mRT}{nF}pH \qquad (1)$$

Where *R* is the gas constant (8.314 J K^{-1} mol^{-1}), *T* is the temperature in K and *F* is the Faraday constant (96485 C mol^{-1}). From equation (1), it can be deduced that the potential varies by the amount -59(*m*/*n*) mV / pH. This means that when the slope has a value around -59 mV / pH, i.e. for pH ≤ 4.24 or pH ≥ 5.33 in the present case, the mechanism involves equal number of

electrons as protons. On the other hand, when the slope has a value around -29 mV / pH, i.e. for 4.24 ≤ pH ≤ 5.33, the mechanism involves twice the number of electrons than protons.

Figure 2

To determine the number of electrons in the electrochemical oxidation of GA, the voltammogram of GA obtained on a microelectrode under steady state conditions was compared to that of 1,1'- ferrocenedimethanol, which exhibits a well-known one electron process (Fig. 3). Irrespective of the pH region (pH ≤ 4.24, 4.24 ≤ pH ≤ 5.33 and pH ≥ 5.33), the electrochemical response of GA is twice that of 1,1'- ferrocenedimethanol, attesting that two electrons are involved in the overall oxidation of GA, whatever the pH. In order to confirm this result, the voltammogram of caffeic acid, which has a similar structure to that of GA and requires the transfer of two electrons [42] has also been recorded and are compared in Fig. 3. The current associated to caffeic acid oxidation (Fig. 3) presents the same intensity as that of GA, corroborating the participation of two electrons during the oxidation step of GA. Thus, based on the slope values analysis from Fig. 2, $2e^-$, $2H^+$ are exchanged at pH ≤ 4.24 and pH ≥ 5.33 while $2e^-$, $1H^+$ are involved for 4.24 ≤ pH ≤ 5.33. A diffusion coefficient of $D = 6.5 \times 10^{-6}$ $cm^2\ s^{-1}$ of GA was calculated from equation (2).

$$I = 4nFCDr \qquad (2)$$

Where I is the steady state current, n is the overall number of electrons transferred, C is the concentration in mol cm^{-3} and r is the radius of the microelectrode in cm.

Figure 3

3.2. The bicubic scheme of GA redox process

Based on the above assessment of e^- and H^+ exchanges at different pH, redox mechanism of GA can be described by a bicubic scheme [35] where electrooxidation steps are written horizontally from left to right and deprotonation steps of the alcoholic functions are presented in downward fashion (Fig. 4). It is made of two simplified 9-members square schemes, in

which the species on the front face (in black) correspond to those protonated on the electroinactive acidic function (COOH), written as Mp to Vp. On the other hand, the species present on the inner face (in red) corresponds to the deprotonated form (COO^-) written as M to P. Both faces are linked by deprotonations of the acidic function COOH (in blue).

Figure 4

Several dissociation constants (pK_a) shown in the bicubic scheme have already been reported (Table 1). Erdemgil et al. [30] determined the first (pK_aV, COOH/COO^-) and the second (pK_a5, OH/O^-) ionization constants by potentiometry and chromatography. Their values are also in good agreement with those reported by Eslami et al. [43] who determined pK_a of the radical species by electron paramagnetic spectroscopy. Herein, different pK_a values of GA are deduced from the extrapolation of intersection points of different linear regimes of Ep versus pH plot on the abscissa (Fig. 5). In other words, the point where slope of the equilibrium diagram changes corresponds to a pK_a value. At pH=4.24, the mechanism changes from a $-2e^-,-2H^+$ process having a slope of -59 mV/ pH unit to a $-2e^-,-1H^+$ reaction with a slope of -29 mV/ pH unit. This pH value corresponds to the first dissociation constant (pK_aV) of the acidic function:

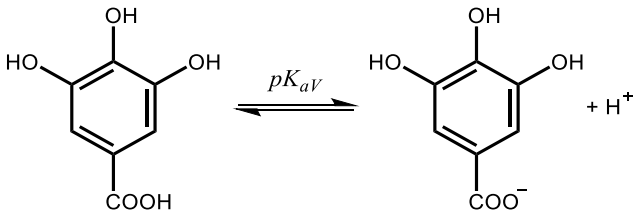

The calculated value fits well to the values previously reported in the literature (Table 1). Indeed, this pK_a of the acidic function could be responsible for the high antioxidant activity of GA [29], since the carboxyl is an electron-withdrawing group [44] that does not promote the

radical scavenging, while the deprotonated carboxyl anion becomes an electron donating group, which promotes radical scavenging by hydrogen atom transfer from the OH functionalities and electron donation [29, 45]. At pH ≤ 4.24, GA is protonated (Vp). It undergoes a $-2e^-,-2H^+$ process to form the ortho-quinone (Mp):

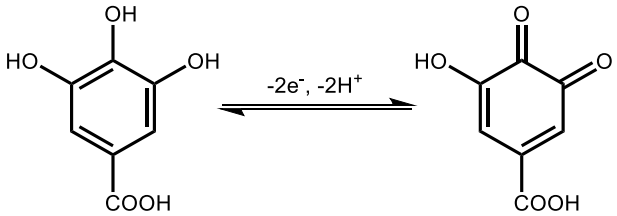

When 4.24 ≤ pH ≤ 5.33, the initial form of GA is deprotonated (V). It undergoes a $-2e^-,-1H^+$ process to form the ortho-quinone (Mp):

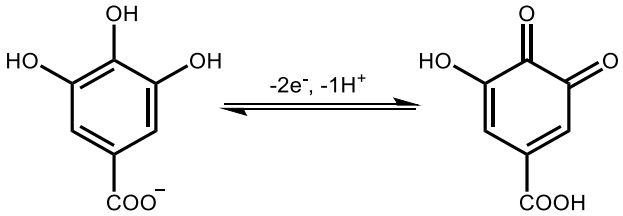

In this pH region, the formation of the ortho-quinone (Mp) with a protonated acidic function was previously reported by HPLC/MS analysis of the products formed after flash photolysis of an aqueous solution of GA [46], which confirms the aforementioned mechanism.

At pH ≥ 5.33, GA is in its deprotonated form (V). It undergoes a $-2e^-,-2H^+$ process to give the deprotonated ortho-quinone (M):

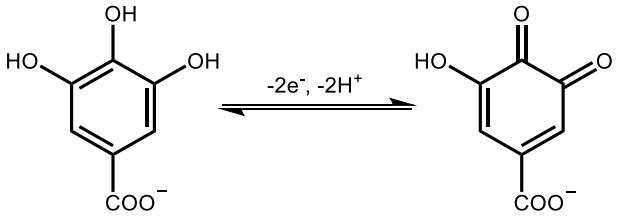

The pH of the transition between the slope of -29 mV/pH and that of -59 mV/ pH corresponds to the dissociation constant of the final ortho-quinone (pK_{aM} = 5.33).

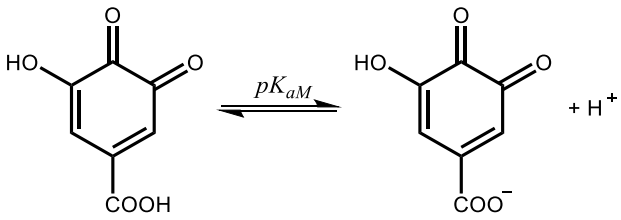

Figure 5

The pK_{a2p} value is not known for GA, but it has been taken equal to -1 for benzoquinone [37] or catechol [38, 39]. Similarly, pK_{a3p} can not be determined here but it was estimated as -6 or smaller previously [37]. Therefore, in this work, we will use pK_{a2p} = -1 and pK_{a3p} = -6. On the other hand, an estimation of the potential difference $(E^0_{4p} - E^0_4)$ is extracted from the slope (ρ = 0.102 V) of the linear correlation between the oxidation potentials of substituted hydroquinones and the Hammett substituent constants, σ [47].

$$\rho = \frac{(E^0_{4p} - E^0_4)}{\sigma_{COOH} - \sigma_{COO^-}} \qquad (3)$$

Here $\sigma_{COOH} = 0.45$ and $\sigma_{COO^-} = 0$,[44] a difference $(E^0_{4p} - E^0_4)$ = 0.046 V is obtained. The same potential difference is also applicable to the quinone and allows calculation of the other pK_as using the equilibrium constants K_i, the Nernst equations and the relationship between them (see for example equations 1-12 of ref. [33]) [33, 35]. Different pK_a values calculated are summarized in Table 1 and are compared with the literature values.

Table 1: pK_a values for GA

Literature results	pK_{aV}	pK_{aP}	pK_{a4}	pK_{a5}	pK_{a2p}	pK_{a3p}
	4 [43] 4.24 [30]	4 [43]	5 [43]	8.7 [43] 8.27 [30]	-1 [37-39]	6 [37]
Our results	pK_{aV}	pK_{aM}				
	4.24	**5.33**				
Calculated results	pK_{aR}	pK_{aN}	pK_{a2}	pK_{a4p}		
	3.5	6.1	-0.5	2.9		

3.3. The spectroelectrochemical study

Spectroelectrochemical study was performed to further validate the formation of different species in each of the three zones: at pH 3 i.e. before pK_{aV}, at pH 5 i.e. between pK_{aV} and pK_{aM} and at pH 6 i.e. beyond pK_{aM}. An electrolysis was conducted at a fixed potential of 0.85 V vs. Ag/AgCl 3 M, which is just after the oxidation peak (Fig. 1) of GA and UV-visible spectra were recorded synchronously. The evolution of the UV-visible spectra in the different pH regions is presented in Fig. 6a-c.

Figure 6

At each pH, the absorption spectrum of GA before electrolysis was recorded, which are compared in Fig. 6d. Notably, the spectrum recorded at pH 3 presents a strong absorption band at 277 nm (ε $6.65x10^3$) that is slightly shifted to lower wavelength at pH 5 (267 nm, ε $6.65x10^3$) and at pH 6 (267 nm, ε $6.95x10^3$), which corresponds to HOMO → LUMO (Π →Π*) transition of GA or its deprotonated form [48, 49]. The position of the band depends on the ionization state of GA, i.e. on the pK_{aV} value. At pH lower than pK_{aV}**,** GA is in neutral form, whereas at pH higher than pK_{aV}**,** the acidic group of GA is deprotonated and induces a shift of the band towards lower values [48, 49]. It was previously reported that plant phenolic compounds show two bands between 200 to 360 nm [48, 50, 51]. However, in the present case, the first band is not accessible, which is assigned to a narrow wavelength window due to buffer solutions [49]. At pH 3, the oxidation of GA induces a decrease of the band at 277 nm and the formation of intermediate bands at 250, 350 and 420 nm that evolve in new bands at 317 and 580 nm. At pH 5, a decrease of the band at 267 nm is followed by the formation of new bands at 317 and 550 nm. At pH 6, the band at 267 nm lowers, while new bands appear at 280, 350 and 545 nm. Interestingly, intermediate species formation is not detectable at pH 5 and 6. Appearance of a

wide peak at wavelengths 310-350 nm was previously reported and was attributed to GA oxidation products [49, 52], the gallate radical and the ortho-quinone. In these studies, the authors demonstrated that the band above 200 nm belongs to the ortho-quinone. It was also reported the formation of oligomers during aerial oxidation of aqueous solutions of GA, revealed by the color change of the initial colorless solution into an orange color and the appearance of a new band at 480 nm [41]. In the present studies, the colorless solution of GA turns into pale yellow at the end of the electrolysis but the final spectra (Fig. 6e) do not reveal the emergence of a new band in this region, which is otherwise characteristic of the dimerization or the oligomerization of GA. We only observed a transient low band at 420 nm at pH 3 that could be attributed to dimerization but it decreases and disappears in the final spectra (Fig. 6a). During the spectroelectrochemical experiment, a purple solid is deposited on the walls of the cell. At the end of the experiment, the adsorption spectrum of the cell emptied of the solution was recorded (Fig. 6f). It reveals a singular broad and symmetric band at 550 nm, which is too high to be attributed to the polymerization of GA. By contrast, it was previously demonstrated by one of us that a one-pot oxidation–co-sublimation solvent-free process of 2-methoxy-1,4-dihydroquinone leads to the formation of a dark violet compound having a strong and broad absorption band centered at 560 nm corresponding to 2-methoxyquinhydrone charge transfer complex [53]. Therefore, it is reasonable to consider that in a cell of thickness 1 mm, the very close presence of GA and its quinone derivative results in the formation of the corresponding charge transfer complex. It is characterized by the evolution of a band in the spectrum in the range of 580 to 545 nm, when the pH increases, in which the band position depends on the ionization states of GA and ortho-quinone. It is important to note that the consumption of 193 mC was obtained, indicating that two electrons per molecule of GA were involved in the oxidation process. This observation, combined with the existence of the band at 317 nm at pH 3 and 5 and of the bands at 280 and 350 nm at pH 6, confirms the formation of the ortho-

quinone. The presence of this quinone and of its hydroquinone (i.e. GA) in a small confined area allows the formation of the charge transfer complex as a purple solid.

3.4. Analysis of the experimental voltammograms

The experimental CV curves were analyzed to extract several kinetic parameters. As a first approximation, the electrochemical response was analyzed using a simple EE process. The Randles-Sevcik equation for a simple irreversible electrochemical reaction (equation (4)) was used to establish the rate-determining step.

$$I_p = 0.446\sqrt{n' + \beta}FCA\sqrt{\frac{nF\nu D}{RT}} \qquad (4)$$

Where I_p is the peak current, *n'* is the number of electrons prior to the rate-determining step, β is the transfer coefficient, *A* is the electrode area in cm^2, *v* is the scan rate in V s^{-1} and *D* = $6.5x10^{-6}$ cm^2 s^{-1}. The variations of the experimental peak current with $v^{1/2}$ were compared with the theoretical values calculated according to equation (4) in which *n'* has been taken equal to 0 to simulate the reaction limited by the first electron transfer (solid lines) or equal to 1 to fit the reaction limited by the second electron transfer (dotted lines) (Fig. 7). They fit well with the solid lines, attesting a rate-limiting step corresponding to the second electron transfer.

Figure 7

Thus, GA oxidation is an irreversible two-electron process, in which the second electron transfer is the rate-determining step. A possible reason for having an irreversible process is the existence of chemical reactions. Thus, in order to fully interpret the voltammetric results, consideration has to be also given to additional chemical reaction(s). Therefore, the variations of the anodic peak potential were analyzed with changing scan rate and the concentration. Fig. 8a depicts the variation of Ep with log*v* at different pH, exhibiting a linear increase of Ep with a positive slope, which are ca. 20 mV. Similarly, the variation of Ep with logC, although of less

significance due to the small range of variation and to the high level of measurement uncertainty, exhibits a straight line with a slope around -20 mV (Fig. 8b).

Figure 8

Such observations of a two-electron irreversible wave support a DISP2 mechanism based on the previous studies [54]. Generally, a DISP mechanism is difficult to demonstrate in buffered media due to the faster proton exchange compared to electron transfer that prevents the DISP reaction to take place [33]. However, we have shown above that the second electron-transfer is the rate determining step. Moreover, it has been demonstrated in the literature that the intermediate semiquinone of GA is stabilized by intramolecular H bonds, involving the two hydroxyl groups [29, 45, 55]. Thus, the unpaired electron in the radical is delocalized over the entire molecule, stabilizing the radical structure. The involvement of the proton in hydrogen bonding with two oxygens in ortho position on the gallate ring was also demonstrated by EPR analysis [43]. The relative stability of the semiquinone should provide sufficient time to the DISP reaction to occur.

Caregnato et al. reported the formation of the phenoxyl radicals by H abstraction from the phenols in aqueous solution using DFT calculations [46]. They confirmed the formation of ortho-quinones and of dimers by recombination of the phenoxyl radicals using HPLC/MS analysis. This was also supported by theoretical calculations and the DISP reaction was expected to be the most favorable pathway. It must be also pointed out that a DISP mechanism was previously demonstrated in the electrochemical oxidation of caffeic acid, a molecule having a structure similar to GA but bearing only two hydroxyl groups [56]. All these arguments corroborate the possibility of a DISP mechanism. To further verify the hypothesis of a DISP2 reaction, a kinetic analysis of GA redox process is performed.

3.5. Kinetic study

The results of the present study has been analyzed using the theoretical treatment of Amatore and Savéant [40], who studied the ECE-DISP mechanism (Scheme 1) and determined the regions of three possible pathways: ECE, DISP1 and DISP2. They summarized their results as a three dimensional kinetic zone diagram (Fig. 9 of ref. [40]), whose axes are the three kinetic parameters of the system: $log\lambda$ ($\lambda = (k_f + k_b)\theta$), $log\lambda_d$ ($\lambda_d = k_d\, c^0\theta$) and $logK$ ($K = k_f/k_b$), where c^0 is the initial concentration in A and θ the time at which the measurement was done.

$A + e^-$ $\overset{E^\circ_1}{\rightleftharpoons}$	B		I
B $\underset{k_b}{\overset{k_f}{\rightleftharpoons}}$	C		II
$C + e^-$ $\overset{E^\circ_2}{\rightleftharpoons}$	D	ECE	III
B + C $\xrightarrow{k_d}$	A + D	DISP	IV

Scheme 1: Different steps of the ECE-DISP mechanism.

The rate determining step in DISP1 is reaction II, while in DISP2 it is reaction IV. We assume that the reaction between two radical species induces electron transfer rather than proton exchange because, if the rate of proton exchange is higher than that of electron transfer, then the DISP reaction will not happen. Let us now designate GA (V or Vp in Fig. 4) by AH_2, and its quinone (M or Mp in Fig. 4) by A. Three reactions between the semiquinone radicals ($A^{-\cdot}, AH^{\cdot}, AH_2^{+\cdot}$) are conceivable, which are shown in scheme 2. It must be noted that the reaction ($2AH^{\bullet} \rightarrow A + AH_2$) is not considered, since it involves proton exchange. The equivalence between our notations and those of Amatore and Savéant [40] are indicated at the bottom of Scheme 2.

Reaction 1	Reaction 2	Reaction 3
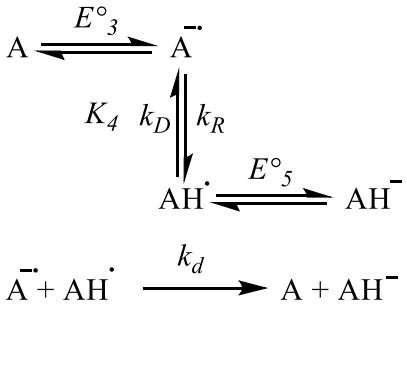	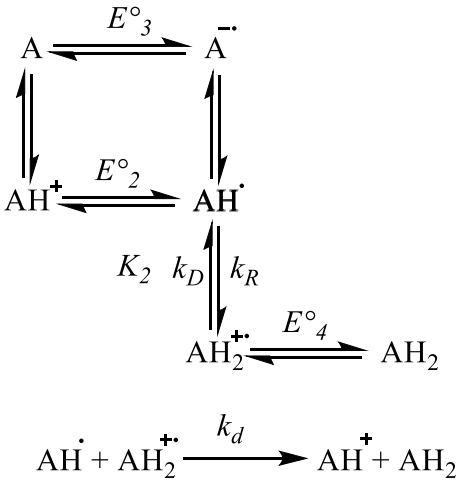	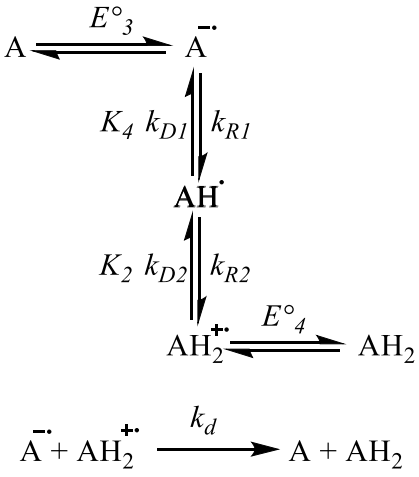
$\boldsymbol{K = \frac{K_{a4}}{c_{H^+}}}$ $\boldsymbol{k_f = k_D}$ $\boldsymbol{k_b = k_R c_{H^+}}$ $\boldsymbol{\lambda = k_R c_{H^+}(1 + \frac{K_{a4}}{c_{H^+}})\theta}$	$K = \frac{K_{a2}}{c_{H^+}}$ $k_f = k_D$ $k_b = k_R c_{H^+}$ $\lambda = k_R c_{H^+}(1 + \frac{K_{a2}}{c_{H^+}})\theta$	$K = \frac{K_{a2}K_{a4}}{c_{H^+}^2}$ $k_f = k_D$ $k_b = k_R c_{H^+}$ $\lambda = k_{R1}k_{R2}c_{H^+}^2 \left[\frac{\left(\frac{K_{a2}K_{a4}}{c_{H^+}^2}+1\right)\theta}{k_{R1}K_{a4}+k_{R2}c_{H^+}}\right]$

Scheme 2: The three different DISP reactions and the equivalence between our constants (right part of the equations) and those defined by Amatore and Savéant (left part of the equations) [40]. For the sake of simplicity, the reactions are written only for the lower square scheme but they can be transposed to the upper one.

The rate of protonation is diffusion limited, therefore $k_R = 10^{11} l\, mol^{-1} s^{-1}$ [57]. The DISP rate constant can be estimated at $k_d = 5.10^9 l\, mol^{-1} s^{-1}$ [58, 59], the time, $\theta = 1s$ and the concentration, $c^0 = 5.10^{-4} M$, giving a value of $log\lambda_d$ = 6.4. The different values of *logK* and $log\lambda$ for the three DISP reactions in the pH range 2-6 are reported in Table 2.

Table 2: Values of *logK* and $log\lambda$ for the different DISP reactions in the pH range 2-6

	Upper square scheme (Protonated species (COOH) in Fig. 4)		Lower square scheme (Deprotonated species (COO^-) in Fig. 4)	
	logK	$log\lambda$	*logK*	$log\lambda$
Reaction 1	-0.9 to 3.1	9 to 8.1	-3 to 1	9 to 6
Reaction 2	3 to 7	12	2.5 to 6.5	11.5
Reaction 3	2.1 to 10.1	11 to 12	-0.5 to 7.5	9 to 11.5

By plotting the values of *logK*, $log\lambda$ and $log\lambda_d$ in the three dimensional kinetic zone diagram (Fig. 9) [40], it can be visualized that reaction 1 (blue and black spheres in Fig. 9) is far from the DISP2 region because *logK* remains too low and that reaction 2 is out of the DISP2 region for the deprotonated species (purple spheres in Fig.9) and at the edge of DISP2 region for the highest values of *logK* when the species are protonated (red spheres in Fig.9). Additionally, in the latter case, the species AH^+ has low probability to exist in the pH range considered due to the high value of pK_{a5}. Conversely, regardless of the state of protonation, reaction 3 can be located in the DISP2 region when *logK* values range from 6.6 to 7.8 (green and orange spheres in Fig.9).

Figure 9

It is thus demonstrated that the use of the ECE-DISP three-dimensional kinetic zone diagram strengthens the results of the CV analysis and the existence of a DISP2 mechanism in the oxidation of GA. Based on this, it is now possible to predict that in reaction 3, the limiting step is the electron transfer between the radical anion and the radical cation of the semiquinone shown in the following reaction:

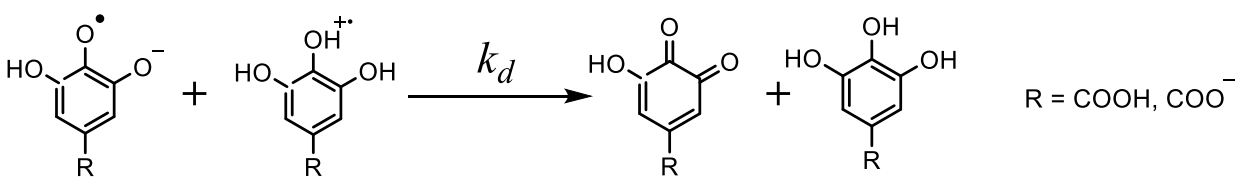

The rate constants are summarized in Table 3.

Table 3: Values used to calculate the different rate constants of the DISP mechanism (See formula in Scheme 2)

pK_{a4}	pK_{a2}	pK_{a4p}	pK_{a2p}	$k_{R1} = k_{R2}$	k_d
5	-0.5	2.9	-1	$10^{11} l\, mol^{-1} s^{-1}$	$5.10^{9} l\, mol^{-1} s^{-1}$

Conclusions

The oxidation of GA in buffered aqueous medium is reexamined in the pH range 1.8-7, which demonstrated that it is an irreversible $2e^-$ process, such that the second electron transfer is the rate determining step. The redox process of GA has been presented systematically through a cubic scheme, involving different electrochemical and chemical steps at different pH. From the analysis of the cubic scheme, different thermodynamics parameters of the redox system are determined in the light of Laviron's theory. In particular, different values of $pK_a s$ are calculated and we report, for the first time, the acidity constant of the ortho-quinone of GA ($pK_{aM} = 5.33$). Spectroelectrochemical studies further sheds light on the generation of different redox species during the GA oxidation at different pH and identify the formation of orthoquinone through a $2e^-$ transfer process as the final product of GA electrooxidation. The analysis of the CV cycles recorded at varying scan rate and concentration suggests the existence of a DISP2 mechanism, which is further confirmed by the kinetic study using the theoretical treatment proposed by Amatore and Saveant for an ECE-DISP mechanism. Our results are reported in the three dimensional kinetic zone diagram. The existence of a DISP2 reaction is clearly demonstrated, in which the limiting step is the electron transfer between the radical anion and the radical cation of the semiquinone. The approach described here allows a deeper comprehension of the oxidation mechanism of GA and will help a better understanding of the

mechanisms involved in the outstanding antioxidant properties of GA in the biochemical environment.

Conflicts of interest

There are no conflicts to declare.

Acknowledgments

The authors thank Université de Bourgogne and European Union to provide financial support through PO FEDER-FSE Bourgogne 2019/2022 (via CoMICS program). A.K. acknowledges Université de Bourgogne for a postdoctoral fellowship through the BQR program.

References

[1] H. Akalın, M. Bayram, R.E. Anlı, Determination of some individual phenolic compounds and antioxidant capacity of mead produced from different types of honey, J. Inst. Brewing, 123 (2017) 167-174.

[2] W. Qu, A.P. Breksa Iii, Z. Pan, H. Ma, Quantitative determination of major polyphenol constituents in pomegranate products, Food Chem., 132 (2012) 1585-1591.

[3] J.F.S. dos Santos, S.R. Tintino, T.S. de Freitas, F.F. Campina, I.R. de A. Menezes, J.P. Siqueira-Júnior, H.D.M. Coutinho, F.A.B. Cunha, In vitro e in silico evaluation of the inhibition of Staphylococcus aureus efflux pumps by caffeic and gallic acid , Comparative Immunology, Microbiol. Infect. Dis., 57 (2018) 22-28.

[4] A.P. Subramanian, A.A. John, M.V. Vellayappan, A. Balaji, S.K. Jaganathan, E. Supriyanto, M. Yusof, Gallic acid: prospects and molecular mechanisms of its anticancer activity, RSC Advances, 5 (2015) 35608-35621.

[5] A. Abdelwahed, I. Bouhlel, I. Skandrani, K. Valenti, M. Kadri, P. Guiraud, R. Steiman, A.M. Mariotte, K. Ghedira, F. Laporte, M.G. Dijoux-Franca, L. Chekir-Ghedira, Study of antimutagenic and antioxidant activities of gallic acid and 1,2,3,4,6-pentagalloylglucose from Pistacia lentiscus. Confirmation by microarray expression profiling, Chem. Biol. Interact., 165 (2007) 1-13.

[6] L.A. BenSaad, K.H. Kim, C.C. Quah, W.R. Kim, M. Shahimi, Anti-inflammatory potential of ellagic acid, gallic acid and punicalagin A&B isolated from Punica granatum, BMC Complement. Altern. Med., 17 (2017) 47.

[7] T. Marino, A. Galano, N. Russo, Radical Scavenging Ability of Gallic Acid toward OH and OOH Radicals. Reaction Mechanism and Rate Constants from the Density Functional Theory, J. Phys. Chem. B, 118 (2014) 10380-10389.

[8] A. de Cristo Soares Alves, R.M. Mainardes, N.M. Khalil, Nanoencapsulation of gallic acid and evaluation of its cytotoxicity and antioxidant activity, Mater. Sci. Eng. C Mater. Biol. Appl., 60 (2016) 126-134.

[9] M. Liu, H. Xie, Y. Ma, H. Li, C. Li, L. Chen, B. Jiang, B. Nian, T. Guo, Z. Zhang, W. Jiao, Q. Liu, T. Ling, M. Zhao, High Performance Liquid Chromatography and Metabolomics Analysis of Tannase Metabolism of Gallic Acid and Gallates in Tea Leaves, J. Agric. Food Chem., 68 (2020) 4946-4954.

[10] X. Wang, J. Wang, N. Yang, Flow injection chemiluminescent detection of gallic acid in olive fruits, Food Chem., 105 (2007) 340-345.

[11] S.G. Dmitrienko, O.M. Medvedeva, A.A. Ivanov, O.A. Shpigun, Y.A. Zolotov, Determination of gallic acid with 4-nitrobenzenediazonium tetrafluoroborate by diffuse reflectance spectrometry on polyurethane foam, Anal. Chim. Acta, 469 (2002) 295-301.

[12] M.-E. Yue, T.-F. Jiang, Y.-P. Shi, Determination of gallic acid and salidroside in Rhodiola and its preparation by capillary electrophoresis, J. Anal. Chem., 61 (2006) 365-368.

[13] M. Badea, F. di Modugno, L. Floroian, D.M. Tit, P. Restani, S. Bungau, C. Iovan, G.E. Badea, L. Aleya, Electrochemical strategies for gallic acid detection: Potential for application in clinical, food or environmental analyses, Sci. Total Environ., 672 (2019) 129-140.

[14] R. Abdel-Hamid, E.F. Newair, Adsorptive stripping voltammetric determination of gallic acid using an electrochemical sensor based on polyepinephrine/glassy carbon electrode and its determination in black tea sample, J. Electroanal. Chem., 704 (2013) 32-37.

[15] N.S. Sangeetha, S.S. Narayanan, A novel bimediator amperometric sensor for electrocatalytic oxidation of gallic acid and reduction of hydrogen peroxide, Anal. Chim. Acta, 828 (2014) 34-45.

[16] J. Chen, Y. Chen, S. Li, J. Yang, J. Dong, In-situ growth of cerium-based metal organic framework on multi-walled carbon nanotubes for electrochemical detection of gallic acid, Colloids Surf. A Physicochem. Eng. Asp., 650 (2022) 129318.

[17] H.V.S. Ganesh, B.R. Patel, H. Fini, A.M. Chow, K. Kerman, Electrochemical Detection of Gallic Acid-Capped Gold Nanoparticles Using a Multiwalled Carbon Nanotube-Reduced Graphene Oxide Nanocomposite Electrode, Anal. Chem., 91 (2019) 10116-10124.

[18] Ç.C. Koçak, Ş.U. Karabiberoğlu, Z. Dursun, Highly sensitive determination of gallic acid on poly (l-Methionine)-carbon nanotube composite electrode, J. Electroanal. Chem., 853 (2019) 113552.

[19] H. Zhao, Q. Ran, Y. Li, B. Li, B. Liu, H. Ma, M. Zhang, S. Komarneni, Highly sensitive detection of gallic acid based on 3D interconnected porous carbon nanotubes/carbon nanosheets modified glassy carbon electrode, J. Mater. Res. Technol., 9 (2020) 9422-9433.

[20] M. Ghaani, N. Nasirizadeh, S.A. Yasini Ardakani, F.Z. Mehrjardi, M. Scampicchio, S. Farris, Development of an electrochemical nanosensor for the determination of gallic acid in food, Anal. Methods, 8 (2016) 1103-1110.

[21] S.A. Shahamirifard, M. Ghaedi, Z. Razmi, S. Hajati, A simple ultrasensitive electrochemical sensor for simultaneous determination of gallic acid and uric acid in human urine and fruit juices based on zirconia-choline chloride-gold nanoparticles-modified carbon paste electrode, Biosens. Bioelectron., 114 (2018) 30-36.

[22] H. Liu, M. Hassan, X. Bo, L. Guo, Fumarate-based metal-organic framework/mesoporous carbon as a novel electrochemical sensor for the detection of gallic acid and luteolin, J. Electroanal. Chem., 849 (2019) 113378.

[23] C. Ye, X. Chen, J. Xu, H. Xi, T. Wu, D. Deng, J. Zhang, G. Huang, Highly sensitive detection to gallic acid by polypyrrole-based MIES supported by MOFs-Co2+@Fe3O4, J. Electroanal. Chem., 859 (2020) 113839.

[24] I. Novak, M. Šeruga, Š. Komorsky-Lovrić, Electrochemical Characterization of Epigallocatechin Gallate Using Square-Wave Voltammetry, Electroanalysis, 21 (2009) 1019-1025.

[25] Z. Yang, D. Zhang, H. Long, Y. Liu, Electrochemical behavior of gallic acid interaction with DNA and detection of damage to DNA, J. Electroanal. Chem., 624 (2008) 91-96.

[26] J.H. Luo, B.L. Li, N.B. Li, H.Q. Luo, Sensitive detection of gallic acid based on polyethyleneimine-functionalized graphene modified glassy carbon electrode, Sens. Actuators B Chem., 186 (2013) 84-89.

[27] R. Abdel-Hamid, E.F. Newair, Electrochemical behavior of antioxidants: I. Mechanistic study on electrochemical oxidation of gallic acid in aqueous solutions at glassy-carbon electrode, J. Electroanal. Chem., 657 (2011) 107-112.

[28] J.L. Beltrán, N. Sanli, G. Fonrodona, D. Barrón, G. Özkan, J. Barbosa, Spectrophotometric, potentiometric and chromatographic pKa values of polyphenolic acids in water and acetonitrile–water media, Anal. Chim. Acta, 484 (2003) 253-264.

[29] H.-F. Ji, H.-Y. Zhang, L. Shen, Proton dissociation is important to understanding structure–activity relationships of gallic acid antioxidants, Bioorg. Med. Chem. Lett., 16 (2006) 4095-4098.

[30] F.Z. Erdemgil, S. Sanli, N. Sanli, G. Oezkan, J. Barbosa, J. Guiteras, J.L. Beltran, Determination of pKa values of some hydroxylated benzoic acids in methanol-water binary mixtures by LC methodology and potentiometry, Talanta, 72 (2007) 489-496.

[31] E. Laviron, Theoretical study of a 1e, 1H+ surface electrochemical reaction (four-member square scheme) when the protonation reactions are at equilibrium, J. Electroanal. Chem. Interfacial Electrochem., 109 (1980) 57-67.

[32] E. Laviron, Electrochemical reactions with protonations at equilibrium: Part II. The 1e, 1 H+ reaction (four-member square scheme) for a heterogeneous reaction, J. Electroanal. Chem. Interfacial Electrochem., 124 (1981) 1-7.

[33] E. Laviron, Electrochemical reactions with protonations at equilibrium: Part VIII. The 2 e, 2H+ reaction (nine-member square scheme) for a surface or for a heterogeneous reaction in the absence of disproportionation and dimerization reactions, J. Electroanal. Chem. Interfacial Electrochem., 146 (1983) 15-36.

[34] E. Laviron, R. Meunier-Prest, Electrochemical reactions with protonations at equilibriumPart 14. The cubic scheme, J. Electroanal. Chem., 324 (1992) 1-18.

[35] R. Meunier-Prest, E. Laviron, Electrochemical reactions with protonations at equilibrium: Part XV. The 2e−, 2H+ bi-cubic scheme, J. Electroanal. Chem., 328 (1992) 33-46.

[36] C. Costentin, M. Robert, J.-M. Savéant, Update 1 of: Electrochemical Approach to the Mechanistic Study of Proton-Coupled Electron Transfer, Chem. Rev., 110 (2010) PR1-PR40.

[37] E. Laviron, Electrochemical reactions with protonations at equilibrium. Part X. The kinetics of the p-benzoquinone/hydroquinone couple on a platinum electrode, J. Electroanal. Chem. Interfacial Electrochem., 164 (1984) 213.

[38] M.R. Deakin, P.M. Kovach, K.J. Stutts, R.M. Wightman, Heterogeneous mechanisms of the oxidation of catechols and ascorbic acid at carbon electrodes, Anal. Chem., 58 (1986) 1474-1480.

[39] Q. Lin, Q. Li, C. Batchelor-McAuley, R.G. Compton, Two-Electron, Two-Proton Oxidation of Catechol: Kinetics and Apparent Catalysis, J. Phys. Chem. C, 119 (2015) 1489-1495.

[40] C. Amatore, J.M. Savéant, ECE and disproportionation: Part VI. General resolution. Application to potential step chronoamperometry, J. Electroanal. Chem., 102 (1979) 21-40.

[41] I.Y. Tóth, M. Szekeres, R. Turcu, S. Sáringer, E. Illés, D. Nesztor, E. Tombácz, Mechanism of in Situ Surface Polymerization of Gallic Acid in an Environmental-Inspired Preparation of Carboxylated Core–Shell Magnetite Nanoparticles, Langmuir, 30 (2014) 15451-15461.

[42] H. Hotta, M. Ueda, S. Nagano, Y. Tsujino, J. Koyama, T. Osakai, Mechanistic study of the oxidation of caffeic acid by digital simulation of cyclic voltammograms, Anal. Biochem., 303 (2002) 66-72.

[43] A.C. Eslami, W. Pasanphan, B.A. Wagner, G.R. Buettner, Free radicals produced by the oxidation of gallic acid: An electron paramagnetic resonance study, Chem. Cen. J., 4 (2010) 15.

[44] C. Hansch, A. Leo, R.W. Taft, A survey of Hammett substituent constants and resonance and field parameters, Chem. Rev., 91 (1991) 165-195.

[45] B. Badhani, R. Kakkar, Influence of intrinsic and extrinsic factors on the antiradical activity of Gallic acid: a theoretical study, Struc. Chem., 29 (2018) 359-373.

[46] P. Caregnato, P.M. David Gara, G.N. Bosio, M.C. Gonzalez, N. Russo, M.d.C. Michelini, D.O. Mártire, Theoretical and Experimental Investigation on the Oxidation of Gallic Acid by Sulfate Radical Anions, J. Phys. Chem. A, 112 (2008) 1188-1194.

[47] P. Zuman, Substituent effects in organic polarography, Springer1967.

[48] C. Cappelli, B. Mennucci, S. Monti, Environmental Effects on the Spectroscopic Properties of Gallic Acid: A Combined Classical and Quantum Mechanical Study, J. Phys. Chem. A, 109 (2005) 1933-1943.

[49] G. Hostnik, J. Tošović, S. Štumpf, A. Petek, U. Bren, The influence of pH on UV/Vis spectra of gallic and ellagic acid: A combined experimental and computational study, Spectrochim. Acta A Mol. Biomol. Spectrosc., 267 (2022) 120472.

[50] M. Friedman, H.S. Jürgens, Effect of pH on the Stability of Plant Phenolic Compounds, J. Agric. Food Chem., 48 (2000) 2101-2110.

[51] M.S. Masoud, A.E. Ali, S.S. Haggag, N.M. Nasr, Spectroscopic studies on gallic acid and its azo derivatives and their iron(III) complexes, Spectrochim. Acta A Mol. Biomol. Spectrosc., 120 (2014) 505-511.

[52] P. Dwibedy, G. R. Dey, D. B. Naik, K. Kishore, P. N. Moorthy, Pulse radiolysis studies on redox reactions of gallic acid: one electron oxidation of gallic acid by gallic acid–OH adduct, Phys. Chem. Chem. Phys., 1 (1999) 1915-1918.

[53] M. Bouvet, B. Malézieux, P. Herson, F. Villain, Self-organization of the 2-methoxyquinhydrone charge transfer complex in polar planes, CrystEngComm, 9 (2007) 270-272.

[54] M. Mastragostino, L. Nadjo, J.M. Saveant, Disproportionation and ECE mechanisms—I. Theoretical analysis. Relationships for linear sweep voltammetry, Electrochim. Acta, 13 (1968) 721-749.

[55] B. Badhani, N. Sharma, R. Kakkar, Gallic acid: a versatile antioxidant with promising therapeutic and industrial applications, RSC Advances, 5 (2015) 27540-27557.

[56] P. Hapiot, A. Neudeck, J. Pinson, H. Fulcrand, P. Neta, C. Rolando, Oxidation of caffeic acid and related hydroxycinnamic acids, J. Electroanal. Chem., 405 (1996) 169-176.

[57] I.D. Clark, R.P. Wayne, Chemical Kinetics, Elsevier, Amsterdam, 1969.

[58] C.P. Andrieux, C. Blocman, J.M. Dumas-Bouchiat, J.M. Saveant, Heterogeneous and homogeneous electron transfers to aromatic halides. An electrochemical redox catalysis study in the halobenzene and halopyridine series, J. Am. Chem. Soc., 101 (1979) 3431-3441.

[59] H. Kojima, A.J. Bard, Determination of rate constants for the electroreduction of aromatic compounds and their correlation with homogeneous electron transfer rates, J. Am. Chem. Soc., 97 (1975) 6317-6324.

Figure captions

Figure 1: Cyclic voltammograms of GA 0.5 mM in BR buffer/EtOH (v/v: 97.5/2.5) + 0.2 M KNO_3 at 100 mV s^{-1}: (a) Influence of the pH and (b) multicycles at pH 3.82. The appearance of a shoulder is indicated by a * sign in both figures.

Figure 2: Variation of the peak potentials of CV of GA with pH recorded in 0.5 mM GA in BR buffer/EtOH (v/v: 97.5/2.5) + 0.2 M KNO_3 at 100 mV s^{-1}. Standard deviation of each potential value are represented with error bar in black color.

Figure 3: Cyclic voltammograms of 0.5 mM GA (red solid line), caffeic acid (blue dashed line) and 1,1'- ferrocenedimethanol (black dash dot dot line) in pH 5 BR buffer/EtOH (v/v: 97.5/2.5) + 0.2 M KNO_3 at 100 mV s^{-1} on a gold microelectrode of 40 µm of diameter at a scan rate of 10 mV s^{-1}.

Figure 4: The bicubic scheme of GA electrooxidation. The left panel shows the structure of each redox state of GA presented in the right panel.

Figure 5: The schematic equilibrium diagram of GA redox process at different pH.

Figure 6: Evolution of UV-Visible spectra during electrolysis performed at a fixed potential of 0.85 V in a 2 mM GA solution in BR buffer/EtOH (v/v: 90/10) + 0.2 M KNO_3 at pH 3 (a), pH 5 (b) and at pH 6 (c). The first (black line) and the last (red line) spectra are in bold. UV-visible spectra obtained before (d) and after (e) the spectroelectrochemical experiments. Absorption spectrum of the purple solid deposited on the walls of the cell after the spectroelectrochemical experiment at pH 5 (f).

Figure 7: Plot of the GA oxidative peak current with $v^{1/2}$ at three different concentrations: 0.05 mM (black squares), 0.1 mM (red circles) and 0.3 mM (blue triangles) at pH 3.16, compared to the Randles-Sevcik predictions calculated from equation (4) for a multistep irreversible process with (n'= 0; n = 2; β = 0.5) (dotted lines) or with (n'= 1; n = 2; β = 0.5) (solid lines).

Figure 8: Variations of the GA peak potentials in BR buffer/EtOH (v/v: 97.5/2.5) + 0.2 M KNO_3: (a) $E_p = f(\log v)$ diagram at C = 0.5 mM in different pH (b) $E_p = f(\log C)$ diagram at pH 3.16 for scan rates (dark squares) v = 10 mV s^{-1} and (red circles) v = 100 mV s^{-1}. Standard deviation of each potential value in (a) and (b) are represented with error bar in the same color as of the symbol and lines.

Figure 9: Three dimensional kinetic zone diagram [40] showing the different regions (DO, ECE, DISP1 and DISP2). The limits of the different DISP reactions are materialized by spheres of different colors: blue for reaction 1 with protonated species, black for reaction 1 with deprotonated species, red for reaction 2 with protonated species, purple for reaction 2 with deprotonated species, green for reaction 3 with protonated species, orange for reaction 3 with deprotonated species. For the sake of clarity, the DISP2 region (dotted lines) and the different spheres are projected into the plane $logK$-$log\lambda_d$.

Figures

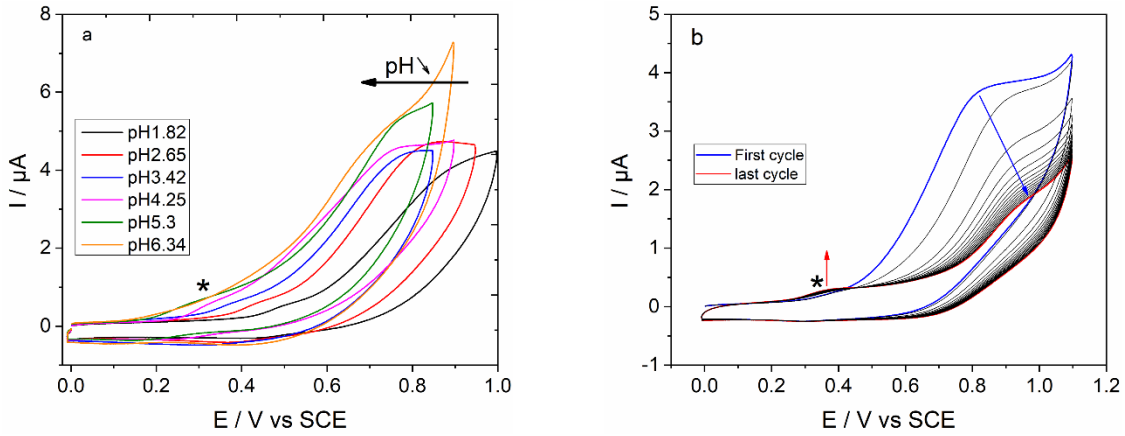

Figure 1: Cyclic voltammograms of GA 0.5 mM in BR buffer/EtOH (v/v: 97.5/2.5) + 0.2 M KNO_3 at 100 mV s^{-1}: (a) Influence of the pH and (b) multicycles at pH 3.82. The appearance of a shoulder is indicated by a * sign in both figures.

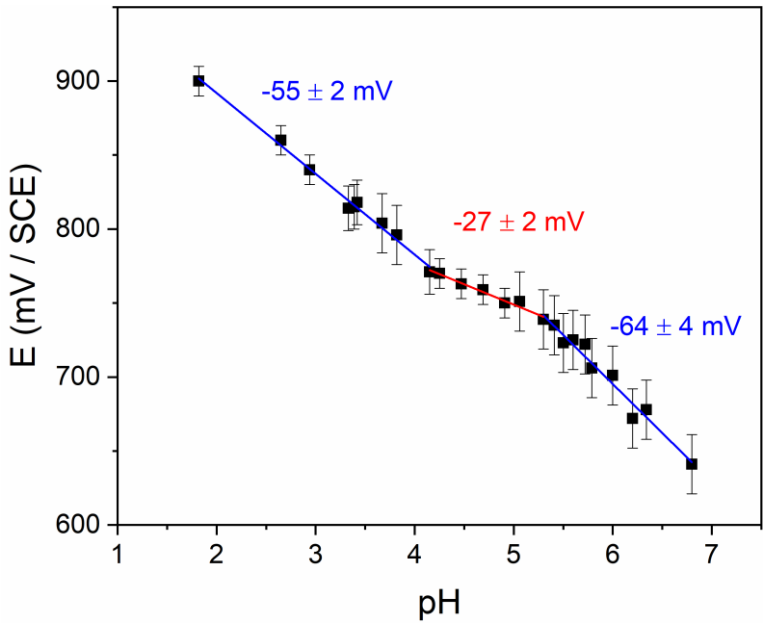

Figure 2: Variation of the peak potentials of CV of GA with pH recorded in 0.5 mM GA in BR buffer/EtOH (v/v: 97.5/2.5) + 0.2 M KNO_3 at 100 mV s^{-1}. Standard deviation of each potential value are represented with error bar in black color.

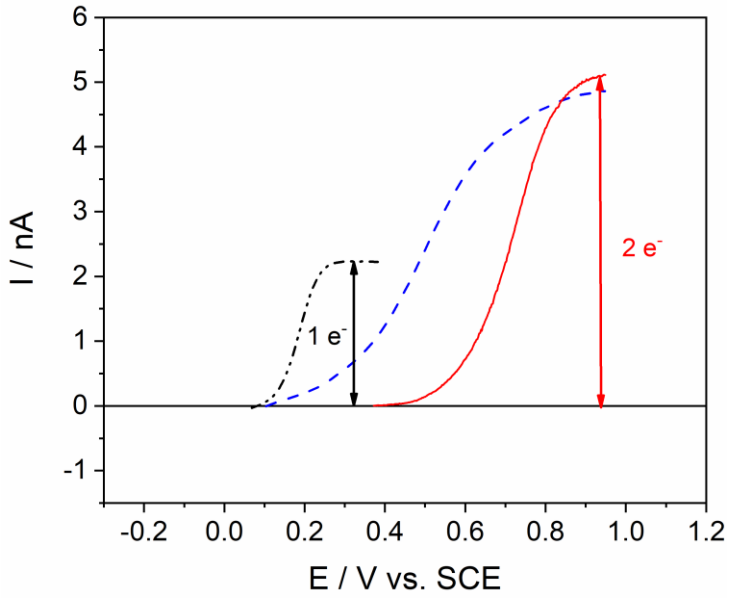

Figure 3: Cyclic voltammograms of 0.5 mM GA (red solid line), caffeic acid (blue dashed line) and 1,1'- ferrocenedimethanol (black dash dot dot line) in pH 5 BR buffer/EtOH (v/v: 97.5/2.5) + 0.2 M KNO_3 at 100 mV s^{-1} on a gold microelectrode of 40 µm of diameter at a scan rate of 10 mV s^{-1}.

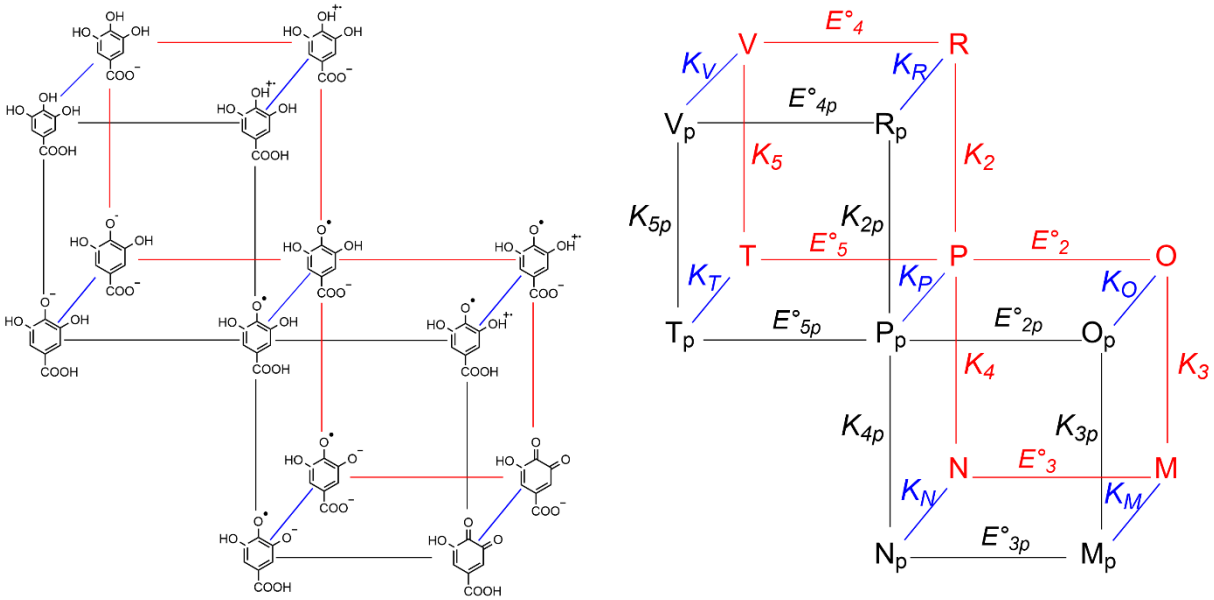

Figure 4: The bicubic scheme of GA electrooxidation. The left panel shows the structure of each redox state of GA presented in the right panel.

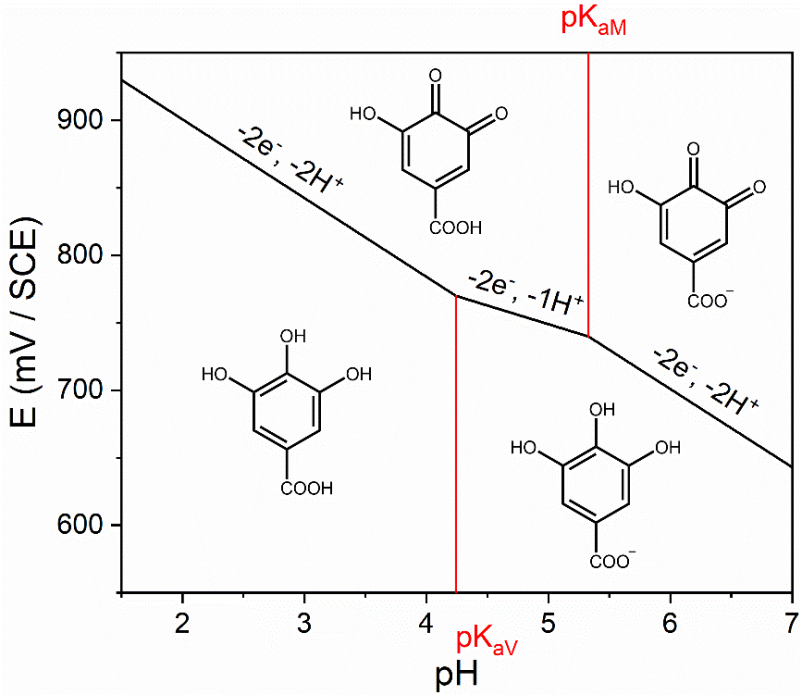

Figure 5: The schematic equilibrium diagram of GA redox process at different pH.

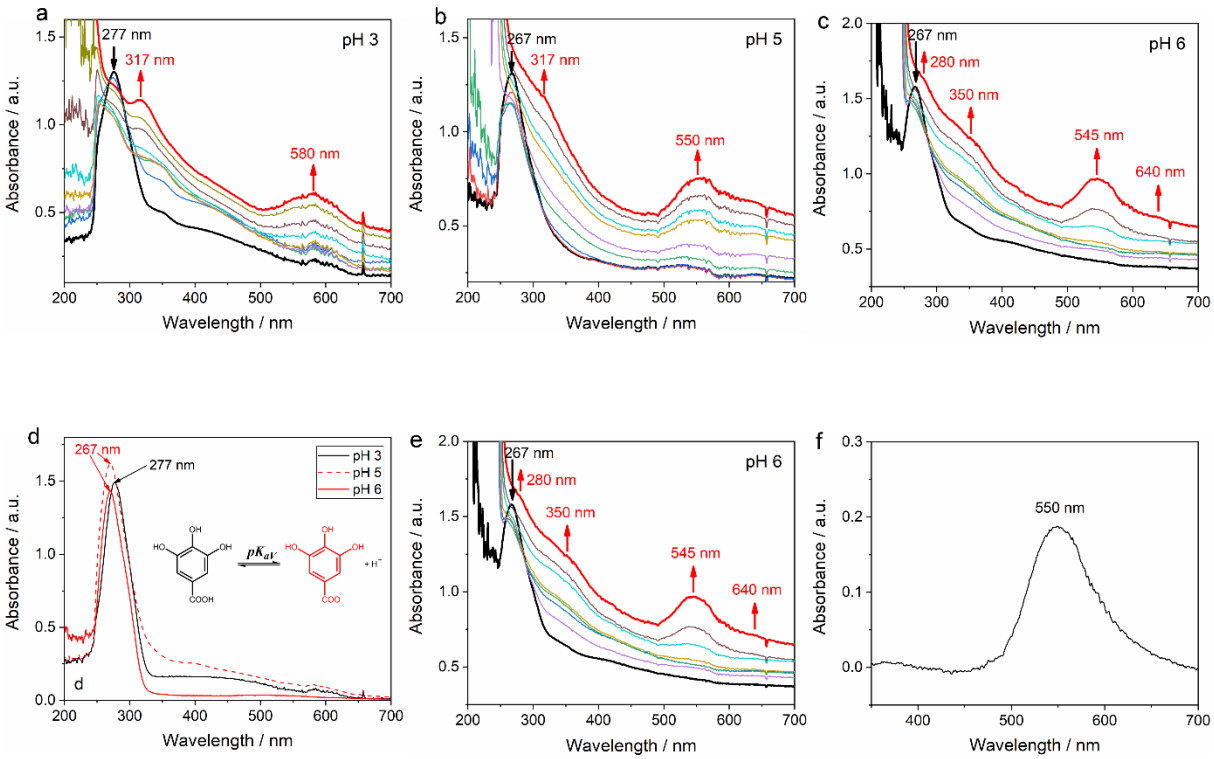

Figure 6: Evolution of UV-Visible spectra during electrolysis performed at a fixed potential of 0.85 V in a 2 mM GA solution in BR buffer/EtOH (v/v: 90/10) + 0.2 M KNO_3 at pH 3 (a), pH 5 (b) and at pH 6 (c). The first (black line) and the last (red line) spectra are in bold. UV-visible spectra obtained before (d) and after (e) the spectroelectrochemical experiments. Absorption spectrum of the purple solid deposited on the walls of the cell after the spectroelectrochemical experiment at pH 5 (f).

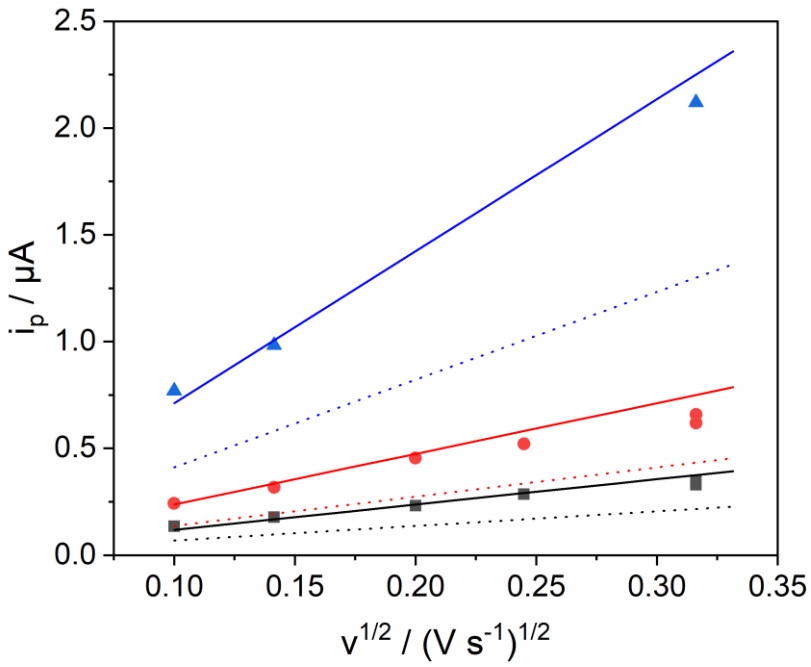

Figure 7: Plot of the GA oxidative peak current with $v^{1/2}$ at three different concentrations: 0.05 mM (black squares), 0.1 mM (red circles) and 0.3 mM (blue triangles) at pH 3.16, compared to the Randles-Sevcik predictions calculated from equation (4) for a multistep irreversible process with (n'= 0; n = 2; β = 0.5) (dotted lines) or with (n'= 1; n = 2; β = 0.5) (solid lines).

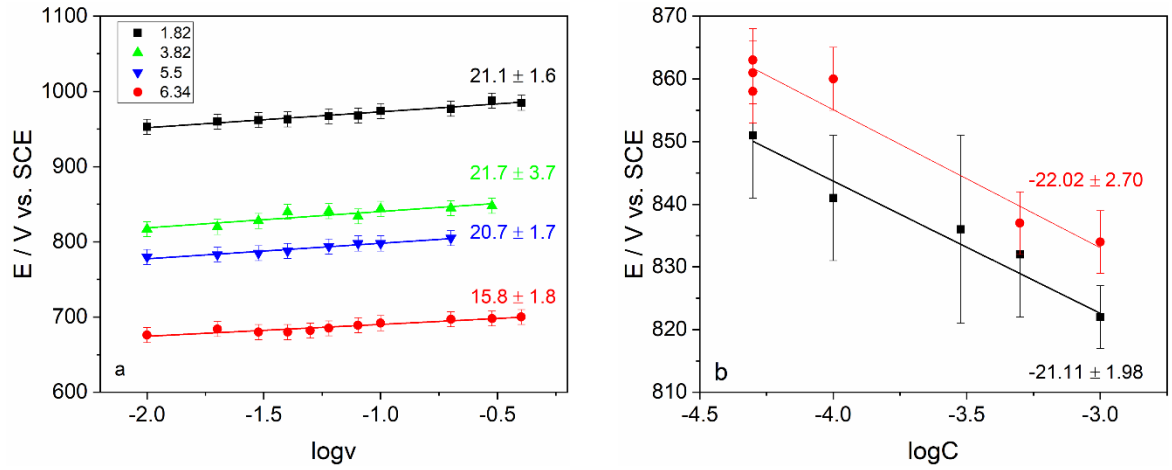

Figure 8: Variations of the GA peak potentials in BR buffer/EtOH (v/v: 97.5/2.5) + 0.2 M KNO_3: (a) E_p = f(log$v$) diagram at C = 0.5 mM in different pH (b) E_p = f(logC) diagram at pH 3.16 for scan rates (dark squares) v = 10 mV s^{-1} and (red circles) v = 100 mV s^{-1}. Standard

deviation of each potential value in (a) and (b) are represented with error bar in the same color as of the symbol and lines.

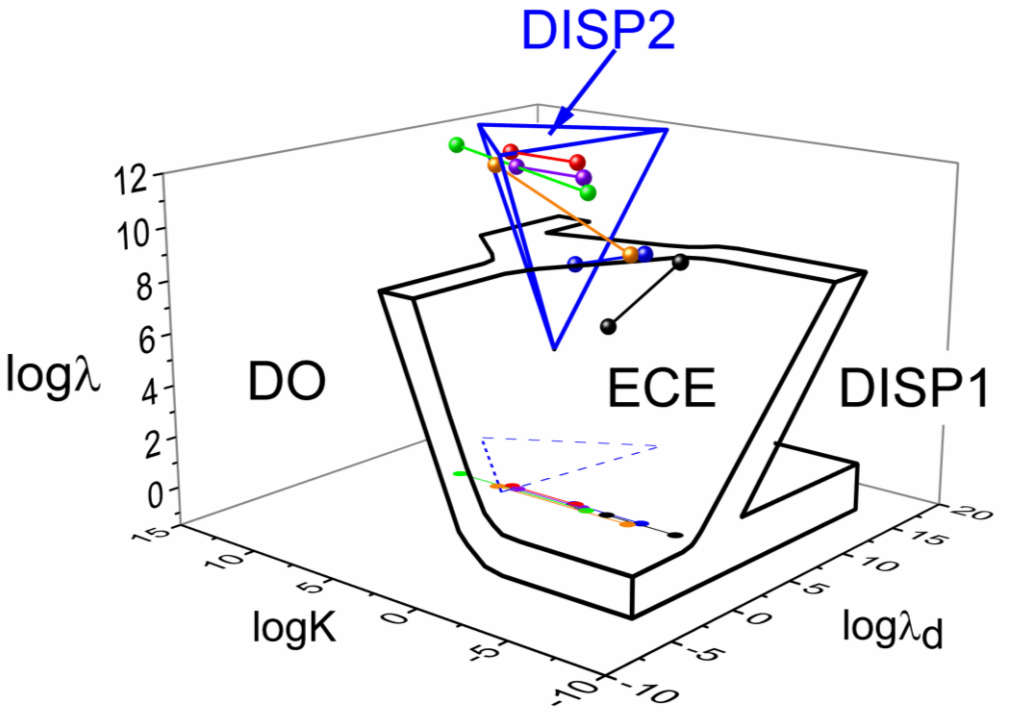

Figure 9: Three dimensional kinetic zone diagram [40] showing the different regions (DO, ECE, DISP1 and DISP2). The limits of the different DISP reactions are materialized by spheres of different colors: blue for reaction 1 with protonated species, black for reaction 1 with deprotonated species, red for reaction 2 with protonated species, purple for reaction 2 with deprotonated species, green for reaction 3 with protonated species, orange for reaction 3 with deprotonated species. For the sake of clarity, the DISP2 region (dotted lines) and the different spheres are projected into the plane *logK-log*λ_d.